

Article

Partial Control and Beyond: Controlling Chaotic Transients with the Safety Function

Rubén Capeáns  and Miguel A. F. Sanjuan * 

Nonlinear Dynamics, Chaos and Complex Systems Group, Departamento de Física, Universidad Rey Juan Carlos, Tulipán s/n, Móstoles, 28933 Madrid, Spain; ruben.capeans@urjc.es

* Correspondence: miguel.sanjuan@urjc.es

Abstract: Chaotic dynamical systems often exhibit transient chaos, where trajectories behave chaotically for a short amount of time before escaping to an external attractor. Sustaining transient chaotic dynamics under disturbances is challenging yet desirable for many applications. The partial control approach exploits the inherent symmetry and geometric structure of chaotic saddles, the topological object responsible of transient chaos, to enable surprising control with only small perturbations. Here, we review the latest findings in partial control techniques with the aim to sustain chaos or accelerate escapes by exploiting these intricate invariant sets. We introduce the fundamental concept of safe sets regions where orbits persist despite noise. This paper presents recent generalizations through safety functions and escape functions that automatically find the minimum control needed. Efficient numerical algorithms are presented and several examples of application are illustrated. Rather than eliminating chaos entirely, partial control techniques provide a framework to reliably control transient chaotic dynamics with minimal interventions. This approach has promising applications across diverse fields including physics, engineering, biology, and more.

Keywords: partial control; transient chaos; escaping orbits

PACS: 05.45.Ac; 05.45.Df; 05.45.Pq



Citation: Capeáns, R.; Sanjuan, M.A.F. Partial Control and Beyond: Controlling Chaotic Transients with the Safety Function. *Symmetry* **2024**, *16*, 338. <https://doi.org/10.3390/sym16030338>

Academic Editor: Branko Dragovich

Received: 18 February 2024

Revised: 2 March 2024

Accepted: 6 March 2024

Published: 11 March 2024



Copyright: © 2024 by the authors. Licensee MDPI, Basel, Switzerland. This article is an open access article distributed under the terms and conditions of the Creative Commons Attribution (CC BY) license (<https://creativecommons.org/licenses/by/4.0/>).

1. Introduction

Chaotic dynamics are widespread in nonlinear systems across diverse fields like physics, engineering, biology, and ecology [1]. Though enabling complex behaviors, chaos also leads to unpredictability and lack of control. Over recent decades, various techniques have emerged to control chaos [2–6], typically by eliminating it entirely and stabilizing fixed points or periodic behaviors. However, in some cases the inherent complexity of chaos provides useful benefits worth preserving. Transient chaos [7] has been shown to provide useful benefits in diverse applications. In lasers and chemical reactions, it can increase efficiency and improve performance [8–11]. In structural and combustion systems, it prevents unwanted resonances [12,13]. In ecology, transient chaos can enable healthy population dynamics [14]. Recent work has also demonstrated techniques to control transient chaos in a model of neuron [15] or a neural network affected by electromagnetic radiation [16].

Sustaining the chaotic behavior in these scenarios can be challenging due to the complexity of chaotic saddles and the influence of disturbances (noise). For chaotic systems, even tiny disturbances become amplified exponentially fast, converting deterministic control schemes ineffective. For these reasons, more robust control techniques that explicitly account for uncertainty are required in the real world.

Here, we provide a comprehensive survey of recent theoretical and computational advances in the emerging technique of partial control, which exploits properties of chaotic saddles to sustain desirable transient chaotic behaviors despite disturbances.

Partial control relies on the existence of embedded safe sets in the region containing the chaotic saddle, where trajectories can be maintained indefinitely through occasional small controls even with disturbances. The sculpting algorithm provides an efficient computational technique to identify these safe sets in any chaotic system by recursively discarding unsafe regions.

Recent promising generalizations using safety functions are introduced, which provide a continuum characterization of the minimum bound of control required for any initial condition [17]. Efficient numerical methods to compute these safety functions are presented and analyzed.

On the other hand, if the aim of the controller is to accelerate the escape of the orbits, we have developed the escape function, a function similar to the safety function but computed to intentionally enable quick escapes from transient chaos regions using minimal interventions [18]. Examples illustrate the power of escape functions to control orbits and force the escape to an external attractor. Combining safety functions and escape functions provide further flexibility in sustaining or escaping transient chaos as desired.

2. Partial Control Method

The partial control concept relies on the existence of special regions called *safe sets* embedded within the phase space containing the chaotic saddle. Informally, safe sets are areas near the saddle where trajectories can be sustained indefinitely through occasional small controls, despite disturbances (noise).

To find safe sets, we assume the dynamics in region Q containing the chaotic saddle can be described by the map:

$$q_{n+1} = f(q_n) + \zeta_n + u_n, \quad \text{with} \quad |\zeta_n| \leq \zeta_0, \quad |u_n| \leq u_0.$$

Here, $q_n \in \mathbb{R}^n$ represents certain phase state of the system, and we assume that the map f acts on a region Q like a horseshoe map. The disturbance ζ affecting the map is considered to be bounded such that $|\zeta_n| \leq \zeta_0$. To be realistic, the control term u is also limited to $|u_n| \leq u_0$.

Without the action of a disturbance and control, nearly all orbits inside Q (except a zero measure set) escape from it after some iterations. However with disturbances present, all orbits eventually escape.

The safe set is defined as the subset $Q_\infty \subset Q$. Any safe point $q \in Q_\infty$ satisfies that the orbit $q_{n+1} = f(q_n) + \zeta_n + u_n$ can be sustained in Q_∞ indefinitely. At each iteration, the control $|u_n| \leq u_0$ is chosen based on $f(q_n) + \zeta_n$ to keep the orbit in Q_∞ .

In recent works [14], a significant advancement was achieved with the development of the *sculpting algorithm*, which provides a general method to numerically compute safe sets in essentially any chaotic system. By recursively discarding unsafe regions of the initial region Q , this algorithm is able to compute Q_∞ (the safe set) several times faster than previous methods. The new procedure of finding the safe set is illustrated in Figure 1. We start selecting the region $Q_0 = Q$ and setting the upper disturbance bound ζ_0 and upper control bound u_0 . The *i*th step of the sculpting algorithm can be summarized as follows:

1. Morphological dilation of the set Q_i by u_0 , obtaining the set denoted by $Q_i + u_0$.
2. Morphological erosion of set $Q_i + u_0$ by ζ_0 , obtaining the set denoted by $Q_i + u_0 - \zeta_0$.
3. Let Q_{i+1} be the points q of Q_i , for which $f(q)$ is inside the set denoted $Q_i + u_0 - \zeta_0$.
4. Go back to the first step, except when $Q_{i+1} = Q_i$, in which case we set $Q_\infty = Q_i$. We call this final region, the *safe set*. If the selected u_0 is too small, then no safe set exists, so a larger u_0 is necessary to obtain the safe set.

In practice, computing the safe set Q_∞ requires a finite grid covering Q_0 , since evaluating an infinite number of points is unfeasible. Using higher grid resolutions yields a more accurate safe set, which typically remains practically unchanged beyond a critical resolution. This algorithm is valid in any dimension. For example in [14], safe sets of one, two, and three dimensions have been computed for the paradigmatic Lorenz system [19].

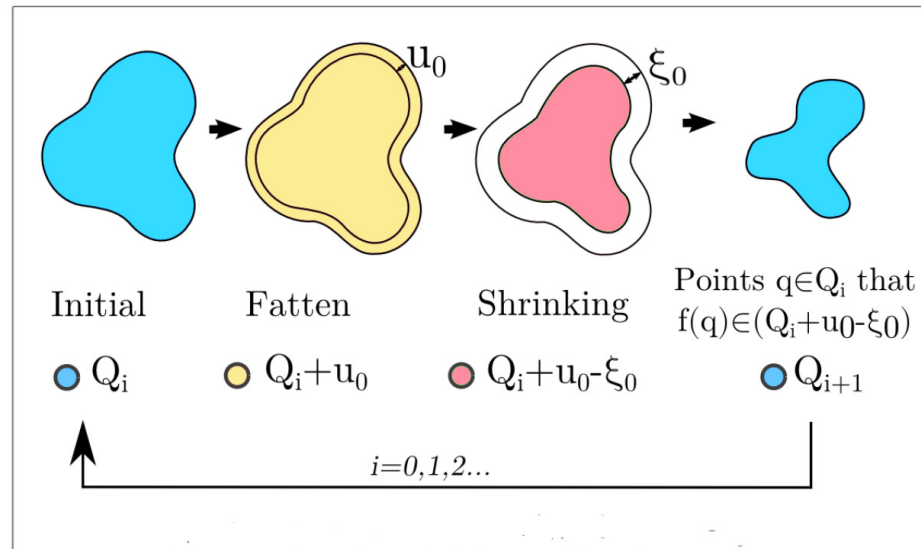


Figure 1. Graphical process used by the Sculpting Algorithm to obtain the safe set.

To show an example of this technique we use the well-known slope-3 tent map. This map is given by:

$$x_{n+1} = \begin{cases} 3x_n + \zeta_n + u_n & \text{for } x_n \leq \frac{1}{2} \\ 3(1 - x_n) + \zeta_n + u_n & \text{for } x_n > \frac{1}{2} \end{cases} \quad (1)$$

and exhibits transient chaos in the interval $[0, 1]$. We consider here that the orbits are affected by an upper disturbance bound $\zeta_0 = 0.040$. An example of an uncontrolled orbit is shown in Figure 2a. To avoid such escapes, we define the region $Q = [0, 1]$ where we want to sustain the orbits and set an upper control bound of $u_0 = 0.025$. We then apply the Sculpting Algorithm to compute the safe set shown in Figure 2b. By forcing the orbit to pass through this safe set, the orbit can be confined in the interval $[0, 1]$ using a control $|u_n| \leq 0.025$ at each iteration. Note that the control bound used is smaller than the disturbance bound ζ_0 affecting the system. However, if smaller values u_0 are used, then no safe set exist, making control impossible.

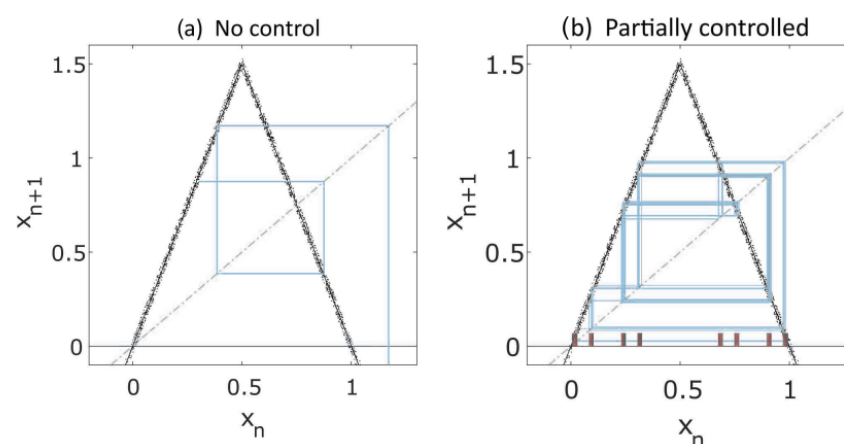


Figure 2. Partial control method. (a) Uncontrolled trajectory under disturbances bounded by $\zeta_0 = 0.04$ (dots) escapes from $Q = [0, 1]$ after a few iterations. (b) Safe set (brown bars at the bottom) computed with upper control bound $u_0 = 0.025$. The orbit is forced through the safe set applying a control $|u_n| \leq u_0$ each iteration. It remains confined to the region $Q = [0, 1]$ indefinitely.

How Safe Sets Depends on ζ_0 ?

A key advantage of the partial control approach is its robustness and adaptability to varying noise intensities. Different noise intensities lead to different safe sets. In a recent work [17] we investigate how the safe set changes for the tent map slope-three (Equation (1)) when it is affected by different upper disturbance bound. In particular, we show in Figure 3 different safe sets for increasing values of ζ_0 in the interval $[0.005, 0, 25]$. For each ζ_0 , we compute the safe set with the minimum control u_0 possible. As can be seen in Figure 3, increasing the disturbance bound ζ_0 results in larger safe sets with fewer partitions. The control u_0 increases nearly linearly with ζ_0 , with a constant ratio of $u_0/\zeta_0 \approx 0.6$. This structure is reminiscent of the Cantor set, a feature typical of nonattracting chaotic sets. A detailed discussion can be found in [17], where we also explore how the safe sets changes with the parameter μ of the map.

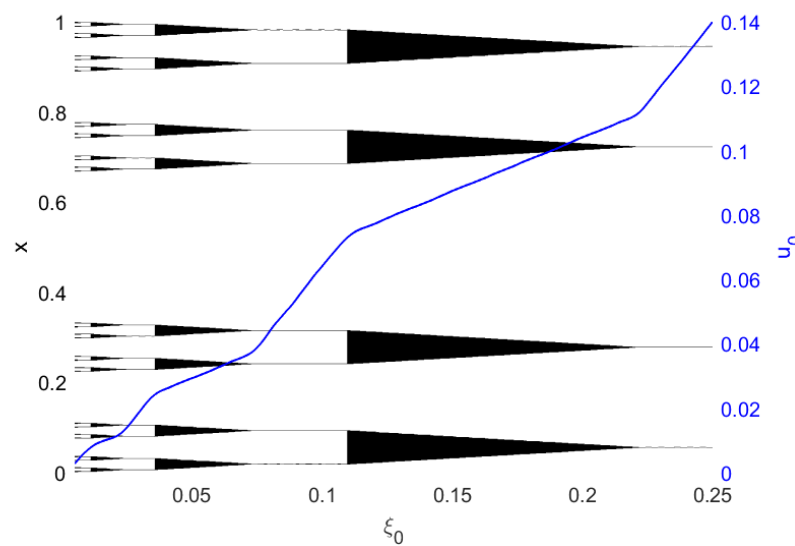


Figure 3. Safe set variation with ζ_0 . Safe sets (black) computed for different disturbance bounds ζ_0 from 0.005 to 0.25, keeping the tent map slope $\mu = 3$ fixed. The corresponding control thresholds u_0 are indicated with the blue line. The ratio u_0/ζ_0 remains near 0.6 as ζ_0 varies.

In [20], we explore also how safe sets changes with the bound of disturbance ζ_0 . However in this work we explore two-dimensional maps. In the first case we use the well known Hénon map for a choice of parameters where the maps exhibits transient chaotic dynamics in the region $Q = [-4, 4] \times [-4, 4]$. The maps are given by:

$$\begin{aligned} x_{n+1} &= a - by_n - x_n^2 + \zeta_n^x + u_n^x \\ y_{n+1} &= x_n + \zeta_n^y + u_n^y. \end{aligned} \tag{2}$$

with $a = 6$ and $b = 0.4$, $Q = [-4, 4] \times [-4, 4]$. $\|\zeta_n^x, \zeta_n^y\| \leq \zeta_0$ and $\|u_n^x, u_n^y\| \leq u_0$.

As shown in Figure 4a,b, when $\zeta_0 = 0.30$, there are 8 thinner strips, and for $\zeta_0 = 0.05$, there are 16 very thin strips.

A similar trend can be seen in the bottom row of Figure 4 that shows the safe sets obtained for the Lozi map for a choice of parameters where transient chaos is present. This map is given by:

$$\begin{aligned} x_{n+1} &= 1 - a|x_n| + by_n + \zeta_n^x + u_n^x \\ y_{n+1} &= x_n + \zeta_n^y + u_n^y \end{aligned} \tag{3}$$

with $a = 2, b = 0.5$, $Q = [-2, 2] \times [-2, 2]$. $\|\zeta_n^x, \zeta_n^y\| \leq \zeta_0$ and $\|u_n^x, u_n^y\| \leq u_0$.

In all cases, the control threshold satisfies $u_0 < \zeta_0$.

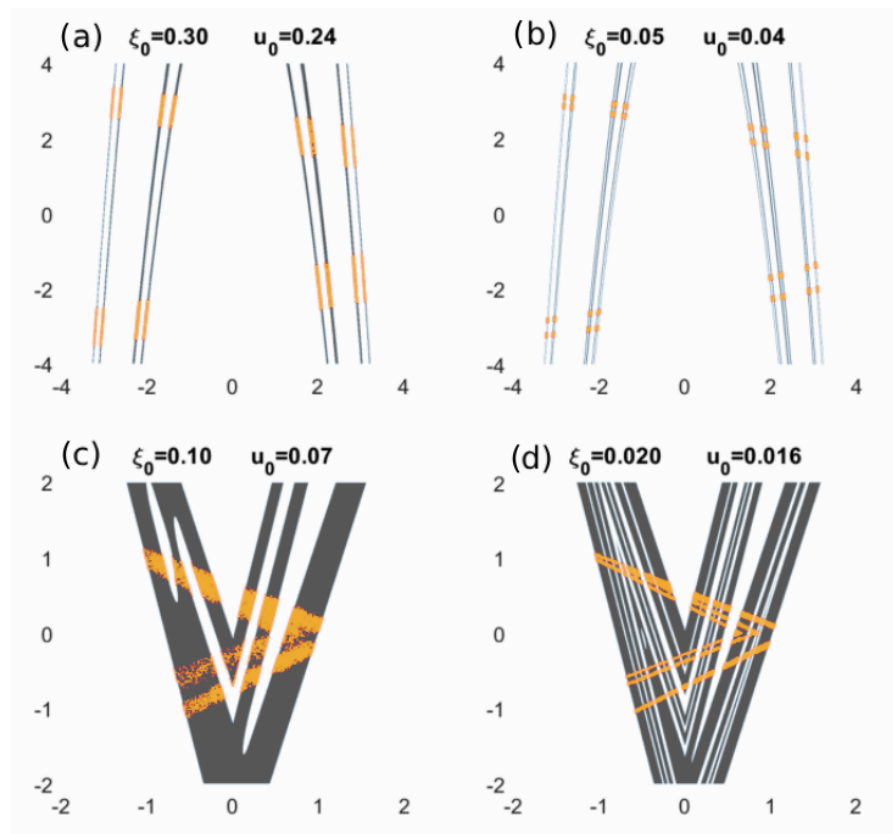


Figure 4. Safe sets (in black) for different ζ_0 . (a–b) safe sets of the Hénon map computed with different upper disturbance bounds. (c–d) safe sets of the Lozi map computed with different upper disturbance bounds ζ_0 . In each case the safe set is computed with approximately the minimum upper control bound u_0 also indicated in the figures. The orange dots represent in each case a controlled orbit (10,000 iterations). The controlled orbit converges to a subset of the safe set called the asymptotic safe set.

Notice that, roughly speaking, the safe set reflects the coarse-grained structure of the stable manifold of the chaotic saddle, being the disturbance ζ_0 the parameter that mainly determines the grain size.

In all the figures we also represent a controlled orbit (orange points) made of 10,000 iterations of the map. As shown the controlled orbit is confined in a subset of the safe set. We call this set the asymptotic safe set. Once the controlled orbits enter in the asymptotic safe set, it remains there indefinitely.

In conclusion, we have shown here that the safe sets are strongly dependent on the disturbance level ζ_0 , which greatly impacts the structure of the controlled orbits. Smaller ζ_0 allows finer control of the orbits. In other words, we show that partial control method takes into account the bound of disturbance affecting the system, producing a suitable safe set to minimize the effort of control.

3. From Sets to Functions

3.1. A Generalization of the Safe Set: The Safety Function

Partial control technique based on safe sets rely on identifying subsets within the phase space region Q where orbits can be controlled with minimal interventions. However, these safe sets only guarantee minimum control for initial conditions starting inside. To generalize this control approach, the novel work [17] introduces the concept of a *safety function* defined across the entire region Q . Rather than a binary classification of ‘safe’ vs ‘unsafe’, the safety

function provides a continuum, indicating how much upper control bound each orbit needs to remain bounded within Q indefinitely. In other words, this function quantifies the control effort required for any initial condition in Q .

3.2. The Computation of the Safety Function

Consider a dynamical system with the goal of sustaining chaotic transients within a phase space region Q , subject to disturbances ξ_n :

$$q_{n+1} = f(q_n) + \xi_n + u_n, \quad (4)$$

where $|\xi_n| \leq \xi_0$. The control challenge is finding a bounded control sequence u_n that contains trajectories within Q indefinitely, while minimizing the upper control bound $u_0 \geq |u_n| \forall n$. Since this value will depend on each initial condition $q \in Q$, we define the function $U(q)$ to be the function that takes the minimum u_0 in each point $q \in Q$.

Due to the chaotic dynamics and the action of disturbances, to find the function U can be challenging. A major breakthrough was realizing that the safety function U can be numerically computed through an iterative calculation process. Specifically, by recursively computing a sequence of intermediate functions U_k that converge over time, one can compute the final function U .

The intermediate function U_k is defined as follows: Given a point $q \in Q$, the value $U_k(q)$ represents the minimum upper control bound necessary to sustain the orbit in Q the next k iterations. In other words, the controlled trajectory starting in the point q , can be sustained in Q during k iterations, by using a control $|u_n| \leq U_k(q)$ in each iteration. The sequence of k controls applied to the trajectory satisfy that $\max(|u_1|, |u_2|, \dots, |u_k|) \leq U_k(q)$.

The recursive algorithm to compute the functions U_k and eventually the function U is as follows:

1. Discretize the region Q into N points $q[i]$.
2. Numerically compute S disturbed images $f(q[i]) + \xi[s]$ for each point.
3. Initialize $U_0(q[i]) = 0 \forall i$ and set $k = 0$.
4. Iterate until convergence:

$$U_{k+1}[i] = \max_{1 \leq s \leq S} \left(\min_{1 \leq j \leq N} \left(\max(u[i, s, j], U_k[j]) \right) \right)$$

(5)

$i \equiv$ index of the starting point $q[i]$, $i = 1 : N$.

$s \equiv$ index of the disturbance $\xi[s]$, $s = 1 : S$.

$j \equiv$ index of the arrival point $q[j]$, $j = 1 : N$.

where $u[i, s, j]$ represents the control applied to the image $f(q[i]) + \xi[s]$ to reach the point q_j , that is, $q[j] = f(q[i]) + \xi[s] + u[i, s, j]$. Typically, for one dimensional maps, values around $N = 2000$ and $S = 20$, are a good trade-off between accuracy and computational cost. More detailed explanation of this algorithm and a the pseudocode can be found in [17].

The step 4 of the algorithm is repeated until it converges, that is when $U_{k+1} = U_k$. This last function is denoted as U which consequently satisfies, $U = U_k = U_{k+1} = \dots = U_\infty$ and therefore the value $U(q)$ provides the upper control bound to sustain the initial condition $q \in Q$ forever (infinite iterations). An orbit starting in q can be sustained indefinitely in Q applying each iteration a control $|u_n| \leq U(q)$.

We can easily relate the safe sets with the safety function. Given the safety function of a map affected by an upper disturbance bound ξ_0 , and selecting an upper control bound $u_0 \geq \min(U)$, the corresponding safe set can be obtained directly as an u_0 -horizontal cut of

the function U . Therefore, the safe set is the subset of points $q \in Q$ that satisfy $U(q) \leq u_0$. The minimum possible upper control bound ($u_0 = \min(U)$), defines the minimum safe set.

3.3. Safety Function for Different Maps

To demonstrate the application of the safety function, we start with a simple example, the slope-three tent map (see Equation (1)) affected by disturbances $|\xi_n| \leq \zeta_0 = 0.06$ (see Figure 5a). For this map, orbits starting in the interval $Q = [0, 1]$ escape after a chaotic transient. In order to sustain indefinitely the orbit in Q , we compute the safety function (drawn in red in Figure 5b) and then we extract the minimum safe set (eight pieces drawn with black small bars on the bottom) that approximately corresponds with $u_0 = \min(U) = 0.04$. In each iteration of the map the control $|u_n| \leq 0.04$ is applied to put the orbit back in the nearest safe point. Controlled orbits in this safe set are shown in gray color. Since the value u_0 selected is the minimum, no other controlled orbits are possible with smaller control bound.

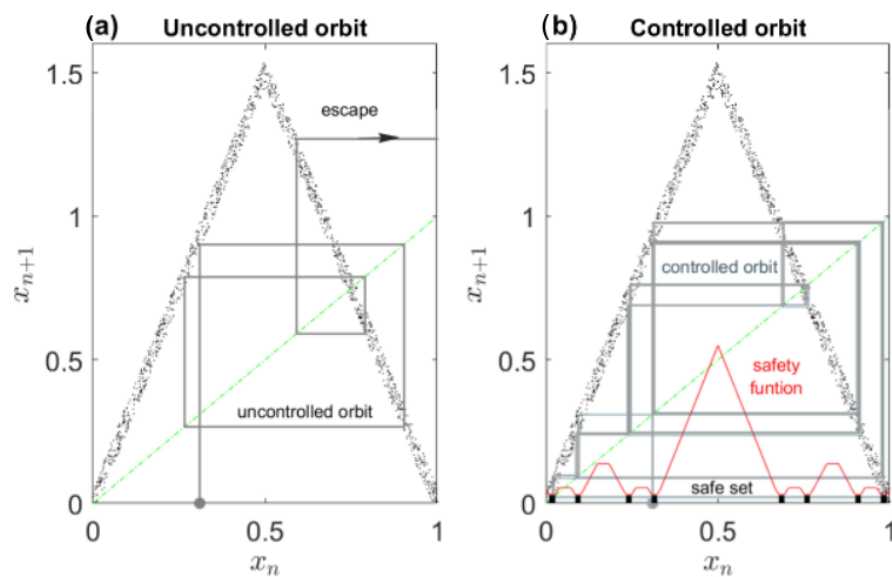


Figure 5. The 1D safety function for the slope-three tent map corresponding to Equation (1). The map is affected by a uniform disturbance bounded by $\zeta_0 = 0.06$. The small dots represent the distribution of the disturbance affecting the map. (a) An uncontrolled orbit escapes from $Q = [0, 1]$ after a few iterations. (b) The safety function in red has 8 minima with value $u_0 = 0.04$. The set of points that satisfied $U(q) = 0.04$ define the minimum safe set represented by the black segments at the bottom. In blue, a controlled orbit. At each iteration, the orbit is forced through the safe set to remain in $Q = [0, 1]$ indefinitely.

We want to remark that the function $U(q)$ is optimal. This means that $U(q)$ gives the smallest possible control bound for each initial condition $q \in Q$. Consequently, no other control strategy can improve on this result by further reducing the control bound. The safety function provides the best possible control policy to keep orbits bounded in Q given the disturbance ζ_0 .

The algorithm to compute the safety functions can easily be extended to maps of higher dimensions. To show that, we take the Hénon map (Equation (2)) and the Lozi map (Equation (3)) shown before, and compute the safety function for a particular upper disturbance bound ζ_0 . The results are presented in Figures 6 and 7. In this case, the safety functions are represented in log scale to enhance the visualization. Notice that the set of points that satisfies $U(q) = \min(U)$ defines the minimum safe set. This set corresponds to the bluest points of the safe sets shown in Figures 6 and 7.

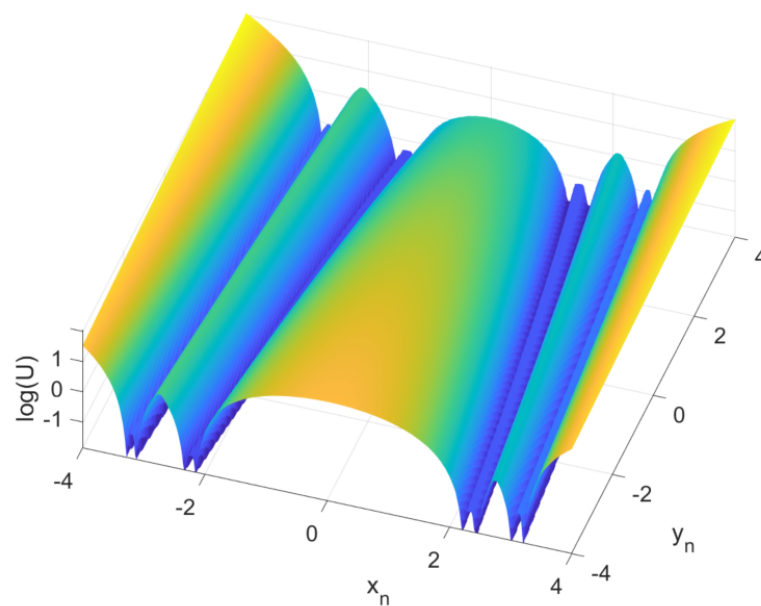


Figure 6. The 2D safety function for the Hénon map corresponding to Equation (2) with disturbance bound $\xi_0 = 0.20$. The safety function is computed on $Q = [-4, 4] \times [-4, 4]$ using a 1000×1000 grid. It converges after 18 iterations of the algorithm.

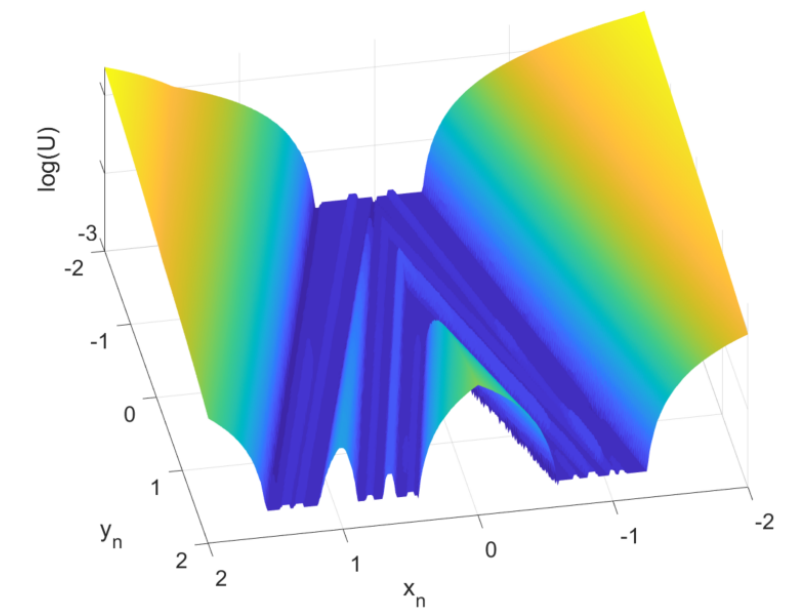


Figure 7. The 2D safety function for the Lozi map corresponding to Equation (3) with disturbance bound $\xi_0 = 0.050$. The safety function is computed on $Q = [-2, 2] \times [-2, 2]$ using a 1000×1000 grid. It converges after 16 iterations of the algorithm.

4. Safety Function to Approach any Orbit to the Safe Set

The introduction of the safety functions enables new potential applications of partial control technique. Perhaps the most notably, it enables controlling orbits from arbitrary initial conditions in Q , not just those confined to the safe set. Here, we present a general strategy based on the safety function to gradually steer any initial condition in Q to the minimum safe set with minimal interventions.

The approach is illustrated using the slope-three tent map (Equation (1)) affected by $\xi_0 = 0.05$ as a classic example of transient chaotic dynamics in the region $Q = [0, 1]$.

For this map, the corresponding safety function U is shown in blue in Figure 8a. As can be appreciated, the function U has 8 minima ($U_{min} = 0.03$). The small regions at these minima represent the smallest possible safe set. In consequence, an orbit in this safe set can be sustained inside Q by applying controls $|u_n| \leq 0.03$ at each iteration of the map. This only applies for initial conditions already inside the safe set. Initial conditions outside, will require larger, but transient, controls to gradually steer the orbit towards the minima of the safety function, where control is minimized.

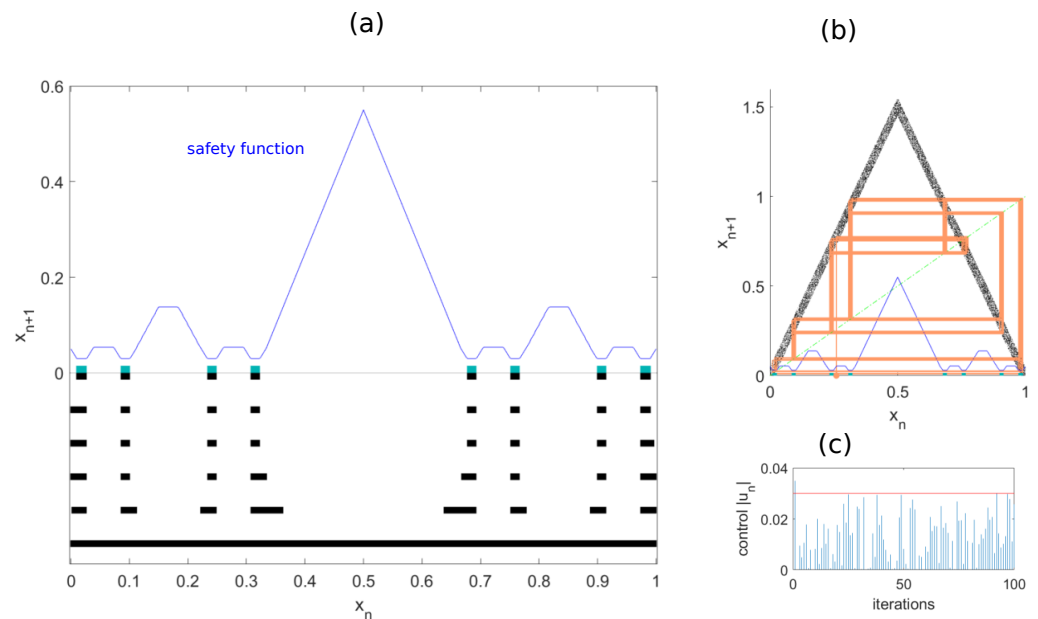


Figure 8. Controlling any initial condition in Q . (a) Black bars show 1000 initial conditions gradually converging to the minimum safe set (green pieces) in at most 6 iterations. (b) A particular controlled orbit (orange line) with the initial condition out of the minimum safe set. (c) First 100 controls $|u_n|$ for the controlled orbit, decreasing as it approaches the minimum safe set. Once inside, controls stay below 0.03.

This gradual approach can be implemented following this control strategy:

1. Given an initial point $q_n \in Q$, evaluate the noisy image $q^* = f(q_n) + \xi_n$.
2. Compute all the possible controls $|u_i| = |q_i - q^*|$ with $q_i \in Q$, being $i = 1 : N$ the grid points in Q .
3. Among all the possible controls, apply the control $u_n = \min \left(\max (|u_i|, U(q_i)) \right)$. The final point will be $q_{n+1} = f(q_n) + \xi_n + u_n = q^* + u_n$.
4. Repeat the algorithm with the new point q_{n+1} .

This approach keep the control as small as possible while the orbit is approaching to the minima of U where the need of control is minimum. As an example we display in the Figure 8a, many controlled orbits for initial conditions in Q . The black horizontal bars (from bottom to top) indicate how starting points progressively move closer to the minima of U . As shown in this case, any initial condition it will take at most six iterations to reach the minima of the safety function (green pieces). In Figure 8b we display an individual controlled orbit that initially starts outside the minimum safe set and gradually approaches to this set. The controls $|u_n|$ applied to this orbit are shown in Figure 8c. Once the orbit reaches the minimum safe set, it remains there forever and the control needed is kept below the value 0.03

To evaluate the effectiveness of our control strategy in guiding different starting points towards the minima of U , we present in Figure 9 the average number of iterations and in Figure 10 the average of control that the orbits need to reach the minima of U . The results are as expected with the exception of the central region of Figure 9, which seems to need a smaller amount of iterations to reach the minima of U . This is due to the fact that the central region maps directly outside Q , especially on the right side beyond Q . Consequently, these points are reintegrated within Q through the application of substantial control, as illustrated in Figure 10 where the central region demands the highest average control.

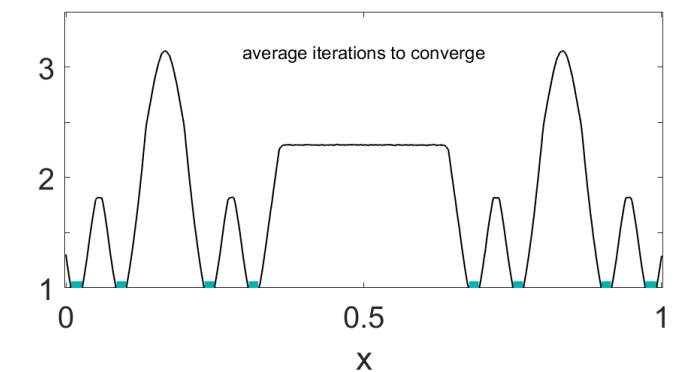


Figure 9. Average number of iterations to reach minimum the safe set. Averaged over 1000 orbits, initial conditions farther from the minimum safe set (green pieces) take more iterations to reach it. The central region is an exception, mapping directly outside $Q = [0, 1]$ to the right. Points here are reinserted into the right side of Q where the safety function is low, so the central area reaches the safe set quickly despite larger controls.

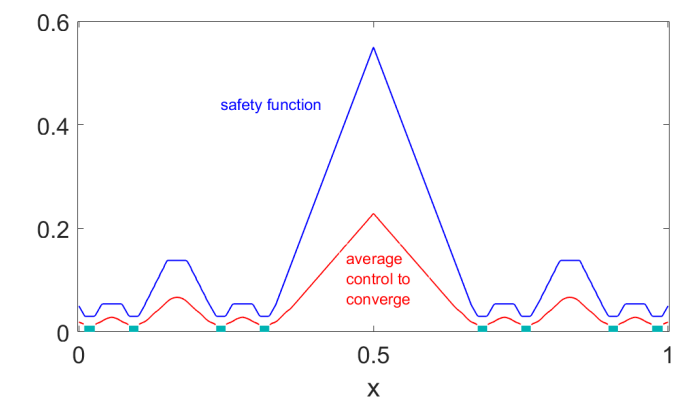


Figure 10. Average control per iteration to reach the minimum safe set. For each orbit, the sum of $|u_n|$ is divided by the number of iterations (1000). The average control shape (red line) resembles the safety function, with initial conditions needing larger control bounds also requiring larger average control.

5. Forcing Controlled Escapes from Chaos

While the partial control technique has traditionally been used to sustain chaotic transients by avoiding escapes, recent theoretical advances have enabled the intentional control of escapes from transient chaos using minimal interventions. This is achieved through the introduction and computation of the new tools *escape functions* and *escape sets*, which allow transforming unpredictable chaotic escapes into predictable controlled exits.

Specifically, consider chaotic dynamics within a region Q modeled by the general nonlinear map:

$$q_{n+1} = f(q_n) + \xi_n + u_n, \quad (6)$$

The key innovation is the formulation of the escape function $U_k(q)$. This function quantifies the upper control bound needed to force orbits starting in the initial condition $q \in Q$, to escape outside the region Q in k iterations or less, despite the presence of disturbances $\xi_n \leq \xi_0$. Correspondingly, for a chosen upper control bound u_0 , the escape set $E_k \subset Q$ can be defined as the subset of initial conditions q where $U_k(q) \leq u_0$. The smaller the u_0 , the smaller the sets E_k . The minimum escape set corresponds to the case $u_0 = \min(U_k)$. Below this value, no escape sets exist.

The summarized steps to apply this control scheme are the following:

1. Select a target iteration N for escape
2. Compute the escape functions U_k for $k = 1 : N$. Select the upper control bound u_0 and extract the corresponding sets E_k .
3. Control the orbit. With initial condition $q \in E_N$, iterate the map $q_{n+1} = f(q_n) + \xi_n + u_n$ and select the suitable $|u_n| \leq u_0$ to move the orbit inside the set E_{N-1} . Iterate again the map and select the suitable $|u_n| \leq u_0$ to move the orbit inside the set E_{N-2} . Repeat the process with E_{N-3} , etc., until the orbit escapes from Q .

To illustrate the capabilities of this escape control framework, three possible scenarios that we consider of interest are presented. The details of the algorithms are shown in [18]. Scenarios I and II are proven with the logistic map

$$x_{n+1} = \mu x_n(1 - x_n) + \xi_n + u_n, \quad (7)$$

where $\mu > 4$ allows the orbits to escape from $Q = [0, 1]$ after a chaotic transient.

- Scenario I: Escape in N or fewer steps. This scenario seeks the fastest escape by allowing the system to abandon the region Q within N iterations or less. By calculating escape functions, we control the trajectory towards escape points within this specified timeframe. This concept is illustrated in Figure 11, while in Figure 11a the logistic map is shown. The escape functions and the corresponding escape sets are displayed in Figure 11b, and Figure 11c shows a controlled escape of an orbit in three or fewer iterations.
- Scenario II: Escape in exactly N steps. Sometimes, a more controlled exit is desired. Here, the system must remain confined within a region for $N - 1$ iterations before escaping at exactly step N . The corresponding functions U_k and sets E_k are shown in Figure 12. Notice that, for this case, the sets E_k , are smaller than before (Scenario I) because the condition of escaping in exactly N iterations is more constrained than escaping in N or less iterations.
- Scenario III: Alternate between transient chaotic regions. Consider a system with a chaotic attractor consisting of two distinct chaotic regions (left and right). without control, the orbit chaotically alternate between both, left and right regions. Imagine we want to dictate how many iterations it spends in each region before switching. As an example, in Figure 13b we display the functions U_k and E_k computed so that the orbit spends three iterations in the right region and two iterations in the left region. A controlled orbit starting in $q \in E_3^r$ follows the sequence $E_3^r \rightarrow E_2^r \rightarrow E_1^r \rightarrow E_2^l \rightarrow E_1^l \rightarrow E_3^r \dots$ repeated. A similar example is shown in Figure 13c, but in this case we impose that the orbit spends 30 iterations on the region right and 20 on the region left. In this case, we do not represent the functions U_k and sets E_k . We only show the time series of the uncontrolled orbit (top panel) and the controlled orbit (middle panel), while in the bottom panel the control used is displayed.

To illustrate the potential of the escape control method, we consider a system with a global chaotic attractor formed by two transient chaotic regions. In this example, the attractor is comprised of two parabola maps as shown in Figure 13a. An orbit, after a few iterations in the region *left* ($0 \leq x \leq 0.5$), escapes to the region *right* ($0.5 < x \leq 1$), and here, after another chaotic transient, it comes back to the region *left*. This produces a chaotic alternation that is repeated indefinitely. The goal is to control the exact number of iterations the orbit spend in each side before change to the

other. This generates a chaotic orbit modulated by a periodic switching. As a simple example, in Figure 13b we display the functions U_k and E_k computed so that the orbit spends three iterations in the *right* region and two iterations in the *left* region. A controlled orbit starting in $q \in E_3^r$ follows the sequence $E_3^r \rightarrow E_2^r \rightarrow E_1^r \rightarrow E_2^l \rightarrow E_1^l \rightarrow E_3^r \dots$ repeated. A more complicated example is shown in In Figure 13c. For this case, the functions U_k and sets E_k were computed to the case of 30 iterations on the region *right* and 20 on the region *left*. We only show the comparison between the uncontrolled orbit (top panel) and the controlled orbit (middle panel), while in the bottom panel is displayed the controls used, always smaller than the upper control bound $u_0 = 0.0135$.

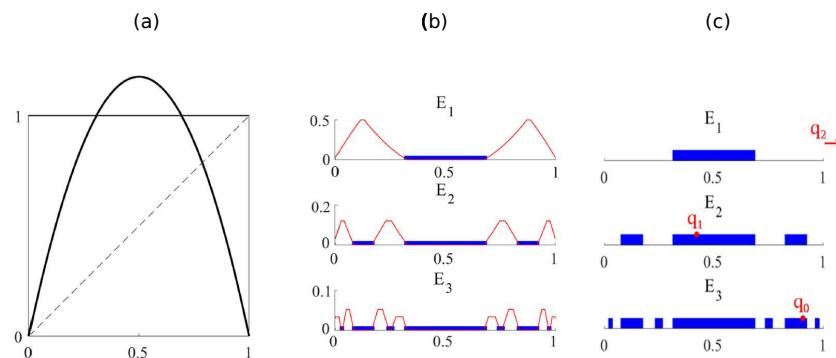


Figure 11. (a) The chaotic dynamics of the logistic map with control parameter $\mu = 4.7$. (b) Escape functions U_k (in red) and escape sets E_k (in blue) are computed for $N = 3$. Orbits starting in E_3 are capable of escaping the chaotic region $Q = [0, 1]$ within three or fewer iterations under the control $|u_n| \leq u_0 = 0.022$. (c) An example of a controlled escape: an initial condition within E_3 is directed towards E_2 , then to E_1 , and ultimately escapes from Q . The escape trajectory and the number of iterations required can vary depending on the initial condition and the noise level ζ_n .

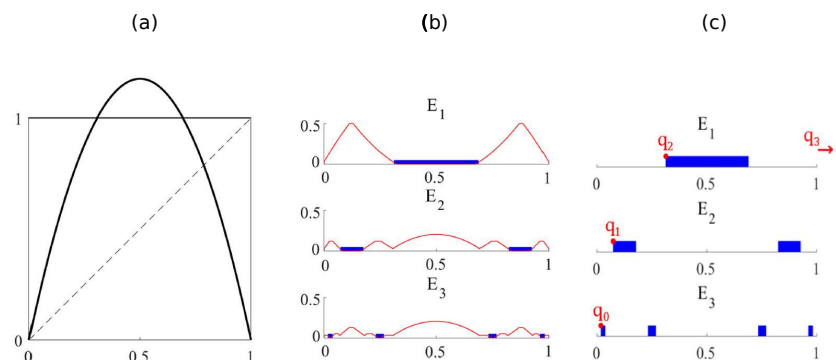


Figure 12. (a) The logistic map with $\mu = 4.7$. (b) The escape functions U_k are computed for $N = 3$ and shown in red. The escape sets E_k are shown in blue. We have used $\zeta_0 = 0.030$ and $u_0 = 0.022$. Orbits starting in E_3 will escape from $Q = [0, 1]$ in exactly 3 iterations with a control $|u_n| \leq u_0$ at each iteration. (c) Example of a controlled orbit. An initial condition in E_3 is mapped to E_2 , then E_1 , and finally it leaves the chaotic region $Q = [0, 1]$ after a suitable control. All orbits starting in E_3 will escape $Q = [0, 1]$ in exactly 3 iterations.

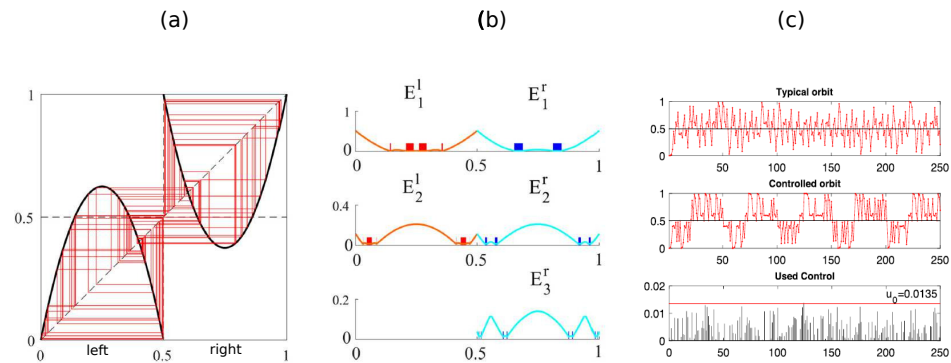


Figure 13. (a) The double parabola map with $\mu = 10$ and the global chaotic attractor in red. Orbits starting in *left* have a transient chaotic behavior before escaping to the region *right* = $[0.5, 1]$ where after another chaotic transient the orbit comes back to *left* = $[0, 0.5]$. (b) The escape functions computed for $N_l = 2$ (orange) and $N_r = 3$ (cyan). Furthermore, the escape sets E^r appear as blue boxes and E^l as red boxes. We have used $\zeta_0 = 0.015$ as the disturbance bound and $u_0 = 0.014$ as the control bound, where this one corresponds to the minimum value of the escape functions. (c) On the top panel, a typical orbit for the double parabola map ($\mu = 10$). In the middle, we show an orbit affected by a disturbance $\zeta_0 = 0.0150$ where we have used an upper control bound $u_0 = 0.0135$ to keep the orbit $N^l = 20$ iterations in region *left* and $N^r = 30$ iterations in region *right*. At the bottom, the absolute value of the control used during the 250 iterations is represented. Note that all the applied controls remain below the control bound $u_0 = 0.0135$ shown by the red line, which corresponds to the minimum value of the escape functions.

6. Conclusions

This paper has provided an overview of recent advances in partial control techniques for sustaining transient chaos. A key foundation described is the concept of safe sets—regions within the phase space where orbits can be confined indefinitely through bounded controls weaker than disturbances. Generalizations using safety functions that directly quantify the minimum control magnitude required for each initial condition further refine this capability. Taking advance of this function, an approach to steer trajectories to the safe set using the safety function with minimal interventions is introduced.

Furthermore, by inverting the traditional goal of partial control, we have introduced the escape functions, designed to intentionally force the escape of trajectories from the region Q in a predictable manner, using small controls. Escape sets based on escape functions enable escaping chaotic regions in precise steps. This new functions expands the potential applications of partial control.

In summary, embracing rather than eliminating chaos, the partial control framework enables predictable control of transiently chaotic dynamics in noisy environments through occasional, tiny perturbations. The demonstrated ability to avoid or force escapes on demand makes partial control a very powerful technique. Besides the use of this method for applications, further theoretical and computational developments should focus on extending these techniques to higher dimensional chaotic systems.

Author Contributions: Conceptualization, R.C. and M.A.F.S.; methodology, R.C. and M.A.F.S.; software, R.C.; writing—original draft preparation, R.C.; writing—review and editing, R.C. and M.A.F.S.; funding acquisition, M.A.F.S. All authors have read and agreed to the published version of the manuscript.

Funding: This research was funded by the Spanish State Research Agency (AEI) and the European Regional Development Fund (ERDF, EU) under Project No. PID2019-105554GB-I00.

Data Availability Statement: Data are contained within the article.

Acknowledgments: I acknowledge the invitation from Branko Dragovich to participate in the 3rd Conference on Nonlinearity at the Serbian Academy of Nonlinear Science.

Conflicts of Interest: The authors declare no conflicts of interest.

References

1. Strogatz, S.H. *Nonlinear Dynamics and Chaos: With Applications to Physics, Biology, Chemistry, and Engineering*, 2nd ed.; CRC Press: Boca Raton, FL, USA, 2015.
2. Ott, E.; Grebogi, C.; Yorke, J.A. Controlling chaos. *Phys. Rev. Lett.* **1990**, *64*, 1196–1199. [[CrossRef](#)] [[PubMed](#)]
3. Pyragas, K. Continuous control of chaos by self-controlling feedback. *Phys. Lett. A* **1992**, *170*, 421–428. [[CrossRef](#)]
4. Shinbrot, T.; Ott, E.; Grebogi, C.; Yorke, J.A. Using chaos to direct trajectories to targets. *Phys. Rev. Lett.* **1990**, *65*, 3215. [[CrossRef](#)] [[PubMed](#)]
5. Braiman, Y.; Goldhirsch, I. Taming chaotic dynamics with weak periodic perturbations. *Phys. Rev. Lett.* **1991**, *66*, 2545. [[CrossRef](#)] [[PubMed](#)]
6. Shinbrot, T.; Grebogi, C.; Yorke, J.A.; Ott, E. Using small perturbations to control chaos. *Nature* **1993**, *363*, 411–417. [[CrossRef](#)]
7. Tél, T. The joy of transient chaos. *Chaos* **2015**, *25*, 097619. [[CrossRef](#)] [[PubMed](#)]
8. In, V.; Spano, M.L.; Neff, J.D.; Ditto, W.L.; Daw, C.S.; Edwards, K.D.; Nguyen, K. Maintenance of chaos in a computational model of thermal pulse combustor. *Chaos* **1997**, *7*, 605–613. [[CrossRef](#)] [[PubMed](#)]
9. Yorke, J.A.; Yorke, E.D. Metastable chaos: The transition to sustained chaotic behavior in the Lorenz model. *J. Stat. Phys.* **1979**, *21*, 263–277. [[CrossRef](#)]
10. Grebogi, C.; Ott, E.; Yorke, J.A. Crises, sudden changes in chaotic attractors, and transient chaos. *Phys. D Nonlinear Phenom.* **1983**, *7*, 181–200. [[CrossRef](#)]
11. De Paula, A.S.; Savi, M.A.; Pereira-Pinto, F.H.I. Chaos and transient chaos in an experimental nonlinear pendulum. *J. Sound Vib.* **2006**, *294*, 585–595. [[CrossRef](#)]
12. Yang, W.; Ding, M.; Mandell, A.J.; Ott, E. Preserving chaos: Control strategies to preserve complex dynamics with potential relevance to biological disorders. *Phys. Rev. E* **1995**, *51*, 102–110. [[CrossRef](#)] [[PubMed](#)]
13. Schwartz, I.B.; Triandaf, I. Sustaining Chaos by Using Basin Boundary Saddles. *Phys. Rev. Lett.* **1996**, *77*, 4740–4743. [[CrossRef](#)] [[PubMed](#)]
14. Capeáns, R.; Sabuco, J.; Sanjuxaxn, M.A.F. Partial control of chaos: How to avoid undesirable behaviors with small controls in presence of noise. *Discrete Contin. Dyn. Syst. Ser. B* **2018**, *23*, 3237–3274. [[CrossRef](#)]
15. López, J.; Coccolo, M.; Capeáns, R.; Sanjuxaxn, M.A.F. Controlling the bursting size in the two-dimensional Rulkov model. *Commun. Nonlinear Sci. Numer. Simul.* **2023**, *120*, 107184. [[CrossRef](#)]
16. Lin, H.; Wang, C.; Tan, Y. Hidden extreme multistability with hyperchaos and transient chaos in a Hopfield neural network affected by electromagnetic radiation. *Nonlinear Dyn.* **2020**, *99*, 2369–2386. [[CrossRef](#)]
17. Capeáns, R.; Sanjuxaxn, M.A.F. Beyond partial control: Controlling chaotic transients with the safety function. *Nonlinear Dyn.* **2022**, *107*, 2903–2910. [[CrossRef](#)]
18. Alfaro, G.; Capeáns, R.; Sanjuxaxn, M.A.F. Forcing the escape: Partial control of escaping orbits from a transient chaotic region. *Nonlinear Dyn.* **2021**, *104*, 1603–1612. [[CrossRef](#)]
19. Lorenz, E. Deterministic nonperiodic flow. *J. Atmos. Sci.* **1963**, *20*, 130–141. [[CrossRef](#)]
20. Capeáns, R.; Sanjuxaxn, M.A.F. Controlling chaotic transients in the Hénon and the Lozi map with the safety function. *J. Differ. Equ. Appl.* **2023**, *29*, 876–884. [[CrossRef](#)]

Disclaimer/Publisher’s Note: The statements, opinions and data contained in all publications are solely those of the individual author(s) and contributor(s) and not of MDPI and/or the editor(s). MDPI and/or the editor(s) disclaim responsibility for any injury to people or property resulting from any ideas, methods, instructions or products referred to in the content.